Gopalakrishnan, Ranjith; Korhonen, Lauri; Mõttus, Matti; Rautiainen, Miina; Hovi, Aarne; Mehtätalo, Lauri; Maltamo, Matti; Peltola, Heli; Packalen, Petteri

Evaluation of a forest radiative transfer model using an extensive boreal forest inventory database

Published in:
Science of Remote Sensing

DOI:
10.1016/j.srs.2023.100098

Published: 01/12/2023

Document Version
Publisher's PDF, also known as Version of record

Please cite the original version:
Gopalakrishnan, R., Korhonen, L., Mõttus, M., Rautiainen, M., Hovi, A., Mehtätalo, L., Maltamo, M., Peltola, H., & Packalen, P. (2023). Evaluation of a forest radiative transfer model using an extensive boreal forest inventory database. *Science of Remote Sensing*, *8*, Article 100098. https://doi.org/10.1016/j.srs.2023.100098

Science of Remote Sensing 8 (2023) 100098

Contents lists available at ScienceDirect

Science of Remote Sensing

journal homepage: www.sciencedirect.com/journal/science-of-remote-sensing

Evaluation of a forest radiative transfer model using an extensive boreal forest inventory database

Ranjith Gopalakrishnan [a,*], Lauri Korhonen [a], Matti Mõttus [b], Miina Rautiainen [c], Aarne Hovi [c], Lauri Mehtätalo [d], Matti Maltamo [a], Heli Peltola [a], Petteri Packalen [d]

[a] School of Forest Sciences, Faculty of Science and Forestry, University of Eastern Finland, P.O. Box 111, 80101, Joensuu, Finland
[b] VTT Technical Research Centre of Finland, PO Box 1000, FI-02044, VTT, Finland
[c] School of Engineering, Department of Built Environment, Aalto University, P.O. Box 14100, 00076, Aalto, Finland
[d] Natural Resources Institute Finland (Luke), Bioeconomy and Environment Unit, Latokartanonkaari 9, FI-00790, Helsinki, Finland

ARTICLE INFO

Keywords:
Radiative transfer modeling
Reflectance
Model validation
Boreal forests
Landsat
Mixed models

ABSTRACT

The forest reflectance and transmittance model (FRT) is applicable over a wide swath of boreal forest landscapes mainly because its stand-specific inputs can be generated from standard forest inventory variables. We quantified the accuracy of this model over an extensive region for the first time. This was done by carrying out a simulation study over a large number (12,369) of georeferenced forest plots from operational forest management inventories conducted in Southern Finland. We compared the FRT simulated bidirectional reflectance factors (BRF) with those measured by Landsat 8 satellite Operational Land Imager (OLI). We also quantified the relative importance of several explanatory factors that affected the magnitude of the discrepancy between the measured and simulated BRFs using a linear mixed effects modelling framework. A general trend of FRT overestimating BRFs is seen across all tree species and spectral bands examined: up to ~0.05 for the red band, and ~0.10 for the near infrared band. The important explanatory factors associated with the overestimations included the dominant tree species, understory type of the forest plot, timber volume (acts as a proxy for stand maturity), vegetation heterogeneity and time of the year. Our analysis suggests that approximately 20% of the error is caused by the non-representative spectra of canopy foliage and understory. Our results demonstrate the importance of collecting representative spectra from a diverse set of forest stands, and over the full range of seasons.

1. Introduction

Forest radiative transfer models use explicit physics-based formulations for simulating the interaction of electromagnetic radiation with the various elements of the forest canopies, other forest layers, tree trunks, and the forest floor. They provide a physically consistent and logical link between the scattering of such canopy elements and satellite observations and can hence help to retrieve forest variables from earth observation data. Indeed, many of the current quantitative global forest canopy products, such as surface albedo and leaf area index (LAI), depend on parametric formulations based on such radiative transfer models (Knyazikhin et al., 1998). These models can be used to differentiate between physically-based causality from indirect (likely spurious) empirical correlation when attributing observed reflectance to canopy characteristics (Knyazikhin et al., 2013; Townsend et al., 2013). Radiative transfer models are also useful for estimating forest and vegetation characteristics in remote locations lacking field plots, as they can be inverted against available remote sensing data (Darvishzadeh et al., 2019; Yang et al., 2010).

Another topical reason for the relevance of such models is their decisive role in understanding the earth's radiation budget and the relative contribution of various land covers, especially in the context of climate change science. Highly accurate reflectance data and simulation is crucial for climate modelling; climate models have stringent minimum sensitivity levels of ±0.02 reflectance units (Schaepman-Strub et al., 2006). Meanwhile, land surface albedo is a critical physical parameter for computing the planetary radiation budget (Chen, 2005), but it remains one of the main uncertainties related to climate modelling (Forster et al., 2007). Reflectance models can also help towards achieving improved, albedo-aware management of boreal forests. This is because various forest management operations such as harvesting and thinning of forest stands influence forest albedo. But there's a lack of methods to

* Corresponding author.
E-mail address: ranjith.gopalakrishnan@uef.fi (R. Gopalakrishnan).

https://doi.org/10.1016/j.srs.2023.100098
Received 20 February 2023; Received in revised form 18 August 2023; Accepted 18 August 2023
Available online 23 August 2023

effectively quantify and incorporate these effects into long-term forest management planning. Forest management planning systems aim at quantifying the climate effects of different management scenarios, but currently ignore the dependencies between forest structure and albedo. Integrating reflectance models into simulations of forest management and growth allows the inclusion of albedo-related climatic effects into practical forest planning.

Although a sizable number of forest radiative transfer models have been developed and described in the past literature, the Forest Reflectance and Transmittance model (Kuusk and Nilson, 2000; Nilson and Peterson, 1991, henceforth FRT) has unique advantages in the boreal zone. It is primarily designed for managed forested stands (Kuusk et al., 2014) and is computationally efficient, especially compared to complex Monte-Carlo ray tracing models such as librat (Disney et al., 2009). So far, it has been validated in the Radiative transfer Model Intercomparison exercises (RAMI, Widlowski et al., 2015; 2007) and in the boreal and hemiboreal zones, using a small set of homogeneous forested stands (Kuusk et al., 2008, 2014; Rautiainen et al., 2008; Hovi et al., 2017). However, it can be parametrized using standard forest inventory data, with the help of relevant allometric equations. The model can simulate the bidirectional reflectance factor (BRF) and the hemispherical directional reflectance factor (HDRF) of a forest stand for any given illumination and viewing geometry, for the wavelength range of 400–2400 nm.

A substantial portion of boreal forests deviate from homogeneous single-species conditions where a majority of previous validation studies have been performed. First, a considerable part of forest area is classified as mixed-species: ~17% in Canada (Natural Resources Canada, 2021) and 46% in Finland (Natural Resources Institute Finland, 2018). There is also considerable variation in understory vegetation in different boreal forest types. Boreal forests commonly have open canopies, where the contribution of forest floor to the satellite-observed BRF is substantial (Rautiainen and Lukeš, 2015). This is especially the case for young forests (e.g., seedling stands before first commercial thinning) with low volume that are common in areas where commercial forestry is practiced in Southern Finland. On mineral soils, the understory vegetation ranges from barren, lichen dominated sites to herb-rich groves. Peatland forests generally have quite open canopies, varied water regimes and soil types, and hence have their own understory vegetation composition that may differ greatly from mineral soils. Further, in boreal forests seasonality affects the reflectance of both overstory and understory vegetation (Rautiainen et al., 2009, 2011; Hovi et al., 2017). Practical applications of forest radiative transfer models require that they can reliably model these variations. Another justification for our study is the fact that previous validation efforts were limited to mature stands. All these reasons motivate the need for validating FRT using in situ observational data over a wide variety of heterogeneous forest conditions, over all age classes (e.g., both young and mature).

A reliable reference dataset is essential for any effort to assess the quality of simulated remote sensing data. The Landsat 8 surface reflectance product is ideal for this purpose as it is based on the Operational Land Imager (OLI) sensor, a high-quality instrument incorporating several technical advancements (Roy et al., 2014). The product itself has been thoroughly validated against other existing products (e.g., MODIS-based) and by similar means over a large number of locations (Vermote et al., 2016). The associated radiometric accuracies of that study showed that it is a high-quality and globally consistent product. Our current work represents one of the first efforts to use this product to assess the accuracy of a physically based radiative transfer model over a large, heterogeneous set of boreal forested areas.

The main objective of this study is to comprehensively and rigorously evaluate the accuracy of the FRT model over a large forest area in the boreal zone, and for different (possibly structurally complex) forest types and seasonal conditions. This is done by using an extensive set of forest field plots and corresponding satellite images from various times of the year (i.e., spring, summer, fall). We take advantage of six years of quality checked Landsat 8 surface reflectance data. The large geographical coverage of the plot data helps us to quantify uncertainties over a wide range of European boreal forest characteristics and seasonal variations. We applied the linear mixed effects model statistical framework (henceforth called mixed models) (Mehtätalo and Lappi, 2020) to help understand the linkage between observed FRT simulation accuracy and probable causes. Such an approach has several advantages, especially given that our goal was to formulate interpretable statistical models, making further inference relatively straightforward. Our specific research questions are: 1) How accurate is FRT in reproducing the observed BRF over a wide range of forested areas? 2) How accurately can FRT reproduce seasonal trends in forest BRF? 3) How much can various forest characteristics (e.g., tree species composition, vegetation heterogeneity and understory type) explain the observed discrepancy between FRT simulations and observed BRFs? By addressing these questions, we aim to identify aspects of the FRT modelling framework where improvements are most pertinent. This will hence pave the way towards better modelling of forest reflectance using stand-level forest inventory data in the boreal zone.

2. Materials and methods

2.1. Study area

The region of our study is Southern Finland, south of the 64°N latitude, approximately bounded by the latitude/longitude based box: (59.7°–64°N) and (21.1°–31.6°E). We concentrated on the southern part of the country for the following two reasons: 1) For more northern latitudes, the uncertainty in satellite-retrieved surface reflectance values increases, mainly because of longer atmospheric paths; 2) The understory vegetation differs at higher latitudes, and there is a lack of understory spectra suitable for FRT. The main tree species found in the study region are Scots pine (*Pinus sylvestris* L.), Norway spruce (*Picea abies* (L.) Karst) and birches (*Betula pendula* Roth and *Betula pubescens* Ehrh). In addition, a few other deciduous tree species such as aspen (*Populus tremula* L.) and grey alder (*Alnus incana* (L.) Moench) may also be present. The understory composition can be variable, depending on the fertility of the site. The most common understory type is mesic, dominated by mosses and dwarf shrubs, such as bilberry (various species in genus *Vaccinium*) and lingonberry (*Vaccinium vitis-idaea* L.). The more fertile sites have an abundance of species including shrubs (e.g., honeysuckle; genus *Lonicera*), ferns, grasses and herbs. Low fertility sites are lichen-dominated, with patches of dwarf shrubs and herbs. We have also restricted our study to months when there is no or negligible snow cover on the ground or trees. This aspect will be elucidated in more detail later (Section 2.5).

2.2. Field plots

We used the publicly available and downloadable forest plot dataset from the Finnish Forest Centre (FFC) (Metsäkeskus, 2022). They are henceforth also referred to as forest plots in this article (for more information, see supplementary materials). The diameter at breast height (DBH), tree height and dominant tree species are available from the plot data. We use following species categories for the plots based on dominant species: “pine group”, “spruce group” and “birch group” (Maltamo and Packalen, 2014), the latter including also other broadleaf species. Henceforth, the tree species of an FFC plot refers to this dominant tree species group.

2.3. Surface reflectance simulations

2.3.1. FRT model

We simulated the plot-level bi-directional reflectance factor (BRF) using the Forest Reflectance and Transmittance (FRT) radiative transfer model. We chose BRF because it corresponds to the only well-validated surface reflectance related product that is available at a forest stand level scale (e.g., 30 m), via the Landsat satellites (more details to follow). The FRT model was first described in Nilson and Peterson (1991) and later significantly modified (Kuusk and Nilson, 2000; Mõttus et al., 2007). The model is classified as a hybrid-type, as it includes characteristics of both geometric-optical and radiative transfer equation-based models. FRT can simulate the BRF and the albedo (bi-hemispherical reflectance) over a given forested scene at a given point in time. The model for the forest canopy contains distinct tree crowns that are approximated by shapes such as ellipsoids. FRT works at the tree class level; there can be up to ten "tree classes", each representing a stratum of similar-sized trees of the same species in a stand. Additional parameters such as the leaf area per tree, needle or leaf clumping index and branch to leaf area ratio further define the structure of the canopy. The scattering elements are assumed to be homogeneously dispersed inside the tree crown envelopes, and the leaf angle distribution is assumed to be spherical. The ground surface is assumed to be covered by a homogeneous layer of understory vegetation. More factors relevant to the simulation (e.g., viewing and illumination geometries, wavelengths simulated) are explained in subsequent sections.

An important element in this context is terminology. In remote sensing based studies, the importance of specifying correctly and unambiguously the directional reflectance characteristics of the primary physical quantity of interest has been stressed (Schaepman-Strub et al., 2006). Our quantity of interest is the Bidirectional Reflectance Factor (BRF), as defined in Schaepman-Strub et al. (2006). It is given by the ratio of the radiance reflected from the surface of interest to that from an ideal and diffuse surface of the same area under identical view geometry and single direction illumination.

2.3.2. Model parameters

Several model input parameters required by FRT were derived from the plot field measurements. In this database of FFC plots, the trees in each plot are divided into a number of strata that contain trees of the same tree species and size class. The "strata" in the plot data correspond to "tree classes" in FRT. Hence, the class-level tree densities (stems ha^{-1}) and median tree statistics (diameter, height) required by the FRT were obtained directly from the plot data and used to simulate the tree stock at each plot. We did not simulate tree size variation within the plot strata. This is a simplification that is close to correct in managed forests that comprised the majority of our area of interest. This is because managed forests are thinned at a height of 10–15 m. Sub-dominant trees are removed in these thinnings, which leaves only the dominant layer where all trees are similar-sized and represent the generation of trees planted after the previous clear-cut. Some structural parameters needed by FRT but not available in the plot data were derived using allometric models or from earlier studies (Table 1). The leaf area index (LAI) was assumed to be constant for all months simulated.

An important input of the FRT model is the reflectance and transmittance spectra of the foliage and bark of the tree species, and of the forest floor vegetation. These were derived from existing spectral databases. For more information, see please refer to the supplementary materials section.

2.4. Reference satellite data

The reference surface reflectance values for each plot were derived from Landsat 8 images. These surface reflectance products are generated using the Land Surface Reflectance Code (LaSRC) for atmospheric correction (USGS, 2020). Details about these algorithms, along with estimates of their accuracy can be found in (Vermote et al., 2016). Landsat surface reflectance products approximate hemispheric-conical reflectance factor; case 8 in Table 2 of (Schaepman-Strub et al., 2006), and are not normalized to any standard geometric configuration. The approximation of hemispheric-conical reflectance factor to BRF is valid under the following conditions: 1) The ratio of diffuse radiation to that of direct radiation is low ("black sky" condition); 2) the hemispherical directional reflectance factor remains constant over the full cone angle of the instrument instantaneous field of view (IFOV). The first assumption is justified, considering that Landsat images are acquired over Finland close to local noon, when the sun is nearest to the zenith position. In clear sky conditions, diffuse radiation is typically less than 10% of the total incoming radiation (Jones and Vaughan, 2010). The second assumption is also justified, considering that the instantaneous field of view is small. Surface reflectance products have been assumed to be approximations of BRF in previous literature; for an example involving the Sentinel-2 satellite data, see Hadi and Rautiainen (2018).

Table 1
Sources used for model parameters specific to the main tree species.

Sl. Num.	Variable name	Values	Reference
1.	Crown base height	From allometric model	Muinonen (1995)
2.	Crown radius	From allometric model	Muinonen (1995)
3.	Dry mass of foliage/leaves (kg)	From allometric model	Pine: eq. A4, Repola (2009); spruce: eq. A10, Repola (2009); birch: eq. 12 in Repola (2008).
4.	Leaf mass per unit area (g/cm^2)	Pine: 158, Spruce: 200, Birch: 57.	Same as Hovi et al. (2016), see Table 3 therein.
5.	Ratio of the branch area to leaf area	Pine: 0.18, spruce: 0.18, birch: 0.15.	Same as Hovi et al. (2016), see Table 3 therein.,
6.	Tree distribution parameter	1.2 (i.e., slightly regular and clustered)	Same as Hovi et al. (2016).
7.	Shoot shading coefficient	Pine: 0.59, spruce: 0.64, birch: 1	Same as Hovi et al. (2016), see Table 3 therein.
8.	Shoot length (m)	Pine: 0.1, spruce: 0.05, birch: 0.4	Same as Hovi et al. (2016), see Table 3 therein.

Table 2
Fixed effects considered for the models. All variables except d_{ms} and SG_{birch} were derived from the FFC plot database; d_{ms} and SG_{birch} were calculated from the satellite image metadata (date of acquisition).

Fixed effect	Variable Name	Description, possible values	Categorical or Continuous
TS	tree species	The dominant tree species (group) for the plot; pine (1), spruce (2) or birch (3).	Categorical
FC	fertility class	Understory type (see Table S2). Can be OMaT (1), OMT (2), MT (3), VT (4), CT (5) ClT (6).	Categorical
ST	soil type	Whether the plot is situated on mineral soil (1), spruce bog (2) or pine bog (3).	Categorical
SG_{birch}	birch state	1 when tree species is birch and DOY >257 (Sep. 14th); otherwise, 0.	Categorical
φ	latitude	Latitude of the plot.	Continuous
h_{msl}	elevation	Height above the mean sea level.	Continuous
V	timber volume	The total volume of timber of the plot.	Continuous
GC_d	Gini coefficient	The Gini coefficient of diameter.	Continuous
H_{sp}	Shannon index	Index quantifying the relative proportion of the three main species is present in the plot.	Continuous
$d_{ms.}$	days to midsummer	The number of days between satellite acquisition date and midsummer (26th June, DOY = 178).	Continuous

2.5. Plot level linking of Landsat and FRT reflectances

This study was restricted to the snow-free months ranging from May to October (both inclusive). This restriction was done partly because of the difficulty on acquiring representative snow spectra over our large region and partly considering that FRT currently does not have an option to account for snow on trees.

We first selected all plots that had been inventoried between the calendar years of 2014 and 2019 (both inclusive) and were south of the 64°N latitude; this yielded a total of 58,344 plots. These calendar years were chosen keeping in mind the availability of Landsat 8 data. We then used the Google Earth Engine (Gorelick et al., 2017) to associate pixels from several Landsat 8 images with each selected plot, if possible. A particular pixel was associated with a plot if.

1. The 30 × 30 m square pixel contained the centre of the plot.
2. There was a maximum of ±6 months temporal difference between the date of measurement of the plot and that of Landsat image acquisition.
3. The Landsat image was acquired between the months of May and October (both inclusive).
4. The pixel was without clouds or cloud shadow effects.
5. Snow was not present in the pixel.
6. The Landsat image was classified as "high quality".

The last three conditions were based on binary flags and metadata that were part of the surface reflectance product; these had been estimated using the Landsat 8 OLI bands (USGS, 2020). We also dropped some plots that were less than 100 m from each other to minimize autocorrelation effects. At this point, we had a set of plots, where each such plot was associated with one or more suitable Landsat 8 pixels. Next, we define an *observation* as an event when a Landsat image acquisition has happened over a given plot. Such an observation is associated with a unique combination of the following.

- A unique FFC forest plot
- A Landsat image, with associated acquisition date and footprint

In all, we had a total of 17,573 such observations after the above screening conditions had been applied. These involved 12,369 unique plots in 5139 L-shaped clusters. These observations had 858 unique Landsat images associated with them.

The viewing and illumination geometries associated with FRT based simulation for each observation are important considerations. The solar azimuth and elevation angles at the plot location for each observation were computed using an open-source solar position code (Reda and Andreas, 2004). Meanwhile, it was assumed that the satellite was directly overhead the plot at that time, hence the view elevation angle was taken as zero. We also assumed a direct illumination ("black sky") condition, with zero sky diffuse lighting. We simulated the BRF (nadir view) of each such observation using FRT, for the wavelengths between 400 and 1700 nm, using 5 nm width bands. The plot measurement data and the sun position associated with the Landsat acquisition were the primary inputs for the FRT model. We also dropped forest strata comprising of very small trees (i.e., those with mean height less than 2.0 m or mean diameter less than 0.5 cm) from these simulations. This was done keeping in mind the ranges associated with the allometric models used.

The wavelength-specific FRT output BRFs were processed into Landsat-8 band specific ones using the relative spectral response curves for the OLI instrument. This was done by taking a weighted average of all FRT (narrowband; 5 nm) bands that mapped onto a given Landsat band. The weighting was based on the spectral response curve of Landsat-8 OLI (Barsi et al., 2014). In this work, we analyzed four of those spectral bands: green (532–590 nm), red (635–673 nm), near infrared (NIR, 850–878 nm) and short-wave infrared 1 (SWIR1, 1566–1651 nm). At this point, we had both the band specific Landsat BRFs and the FRT simulated ones for each of the 17,573 observations.

2.6. General trends in accuracy

We first compared FRT simulated BRFs with Landsat-measured ones, for the summer months (June, July and August) using a set of scatter-plots. The statistical significance of the observed discrepancies (over-estimation or underestimation) was tested by using linear mixed effects models, keeping in mind the grouped structure of the underlying data (explained in detail later).

We then examined the temporal trends in both simulated and observed BRF values using a selected set of FFC field plots. These plots were selected such that each had a temporal series of Landsat images associated with them. In other words, they were such that for each plot, Landsat images were available over it for all snow-free months (May to October) for any particular year (year could be any between 2014 and 2019). That is, only plots that had at least one observation for each of the six months in any particular year were selected for this analysis. When multiple observations were available for a month, one of them was arbitrarily chosen. Then, for each such observation, an FRT simulation was done using the same illumination geometry as the associated Landsat image. The forest stand characteristics for the simulation were obtained from the associated plot characteristics. The selected set of plots were categorized based on dominant tree species and volume of timber. Then, the average BRF (both FRT simulated and Landsat based) was calculated for each category and for each month. These averages were then analyzed as band-specific seasonal trajectories of different forest types in the study area.

2.7. Statistical analysis

For each observation, we computed the difference between Landsat-measured and model-simulated BRF which we henceforth call the error in BRF simulations in the Landsat 8 red and NIR bands as:

$$e_{Red} = BRs_{NIR,\ FRT} - BRF_{NIR,\ Landsat} \tag{2}$$

Where e_{Red} and e_{NIR} denote the error in the red and NIR bands, respectively; $BRF_{Red,\ FRT}$ and $BRF_{NIR,\ FRT}$ represent the BRFs simulated by FRT in the respective bands, and $BRF_{Red,\ Landsat}$ the $BRF_{NIR,\ Landsat}$ are the BRFs observed by the Landsat 8 satellite.

We developed a set of linear regression models linking the error in BRF simulations with several potential explanatory factors to attribute the observed error to probable causes, and to estimate the relative importance of these causes. Our dataset of observations had a distinct grouped structure, with several grouping factors; the grouping is in parameter-space. We had several observations associated with each plot, which is similar to a repeated-measures experiment design. Moreover, it is important to factor in the grouping structure of Landsat images: each image is associated with a unique atmospheric condition and associated atmospheric correction artefacts. Several observations (from several forest plots) may be associated with each such image. We used mixed models, which provide a statistically sound framework to analyze such grouped data, especially when the sample sizes in some groups may be small (Mehtätalo and Lappi, 2020). Mixed models are easier to work with, compared to alternatives such as nonlinear mixed-effects models and hierarchical Bayesian models. We analyzed only the red and NIR Landsat bands in detail, using mixed models because these two bands are a parsimonious set that adequately characterize the crucial aspects of vegetation reflectance. For vegetation, red correlates with other visible bands, and NIR correlates with other infrared bands. Meanwhile, these bands are not strongly correlated with each other (Jones and Vaughan, 2010).

A general matrix-based form of a mixed model where e_{Red} and e_{NIR} are the dependent variables, while forest plot characteristics are used as independent variables, is as follows:

$$\mathbf{y} = \mathbf{X}\beta + \mathbf{Zb} + \varepsilon \tag{3}$$

Where $\mathbf{b} \sim \mathrm{N}(\mathbf{0}, \mathbf{G})$, $\boldsymbol{\varepsilon} \sim \mathrm{N}(\mathbf{0}, \mathbf{R})$, and cov $(\mathbf{b}, \boldsymbol{\varepsilon}) = \mathbf{0}$.

Where, $\mathbf{y}$ is a vector of error values in a given band (e_{Red} or e_{NIR}) associated with n observations, $\mathbf{X}$ is the $n \times p$ design matrix for the p fixed effects (independent variables), and $\boldsymbol{\beta}$ is a $p \times 1$ vector of coefficients associated with the p fixed effects, $\mathbf{Z}$ is an $n \times q$ design matrix for the q random group effects, $\mathbf{b}$ is a $q \times 1$ vector of random group effects and $\boldsymbol{\varepsilon}$ is the $n \times 1$ vector for the residual errors (Mehtätalo and Lappi (2020). Further, $\mathbf{G}$ and $\mathbf{R}$ are variance-covariance matrices: $\mathbf{G} = \mathrm{var}(\mathbf{b})$; $\mathbf{R} = \mathrm{var}(\boldsymbol{\varepsilon})$.

We used the *lme4* package (Douglas Bates et al., 2015) in the R environment to formulate and estimate the coefficients $\boldsymbol{\beta}$ and $\mathbf{b}$ of the mixed models. Separate models were formulated for the mean error in the red band (mod.meanerr.red) and the NIR band (mod.meanerr.NIR). Models were formulated as described in Mehtätalo and Lappi (2020). All fixed effect predictor variables were scaled and normalized before being tried out in the models: we scaled them so that their mean was 0.0 and standard deviation was 1.0. This was done to make the inter-comparison between their associated coefficients possible.

Categorical variables were added as dummy variables, representing each class. For soil type (ST), categories 2 and 3 denote that the plot is on peatland soil. Further, $ST_{type\,=\,1}$ denote the categorical dummy variable indicating whether the plot is situated on mineral soil (i.e., values 0, 1), etc. For tree species (TS), the birch group is dominated by the birches, but a few other broad-leaved trees may also be present. Further, $TS_{sp\,=\,1}$ denote the categorical dummy variable indicating dominance by pine group (i.e., values 0, 1), etc. Fertility classes (FC) 5 and 6 are clubbed into a single level, "5". Moreover, $FC_{class\,=\,1}$ denote the categorical dummy variable indicating fertility class 1 (i.e., values 0, 1), etc. The categorical variable birch state (SG_{birch}) was introduced to factor in a significant discontinuity in the birch leaf spectra; i.e., between *Spec_lateAugust* and *Spec_earlyOctober* (Table S1). The latitude (φ) of the plot was included as a fixed effect, to factor in north-south effects. We included the volume of timber (V), as it is a proxy for the stem density and maturity level of the trees. The gini coefficient of diameter (GC_d) was got by applying the R ineq function in the ineq package (Zeileis & Kleiber, 2014) to the diameter of trees. Values range from 0 (all trees are of the same diameter) to 0.5 (there is considerable variation in the diameter of trees). The shannon index (H_{sp}) quantifies the species diversity of the plot; we consider only the three species groups in this case. The index was computed using the R *diversity* function in *vegan* package (Oksanen et al., 2022). Values ranged from 0 (when there is only one species present) to 1.1 (ln (3); all three species types are present in equal tree count). The value of d_{ms} (days to midsummer) was obtained by the formula: (DOY – 178), where DOY is day of year. This was used mainly to account for the facts that all our understory spectra are from summer.

The mixed models were formulated in the following way. First, we formulated a version of the model that included all fixed effects we considered possible (Table 2). We also considered two interactions, one between the tree species and fertility class (TS:FC) and another, between the gini coefficient of diameter and the dominance of spruce trees (GC_d: $TS_{sp\,=\,2}$). Subsequently, we identified and discarded those fixed effects and interactions that were statistically insignificant; i.e., the p-value associated with their likelihood ratio test (Pinheiro and Bates, 2006) was more than 0.05.

Similarly, several random effects were initially included (Table 3). The plotID accounts for the fact that some plots are observed by Landsat several times. The clusterID is incorporated because each plot belongs to a particular L-shaped clusters. The imageID is unique for each Landsat image (typically 185 × 185 km), which might cover a large number of forest plots. The grouping by imageID is done so that Landsat image specific atmospheric effects, and other such artefacts are taken into account. Even though atmospheric correction is carried out on all images, related artefacts can still be present. Lastly, provinceName takes into account of the fact that our study area in southern Finland consists of 17 administrative provinces. This thus accounts for some local geographic effects. A random effect was subsequently discarded if they explained less than 5% of the residual variance. This threshold was arbitrary; the discarding was done so that the final mixed models would be as parsimonious as possible. Random effects were only included as random intercepts. Further, they were added as crossed effects, with respect to each other. The marginal and conditional R^2 values associated with the final models were computed by using the method of Nakagawa and Schielzeth (2013). The significance of the random variables were estimated by computing the percent of residual variance explained by them.

2.8. Relative contributions of spectral and geometrical components

In general, the magnitude of error associated with an FRT reflectance simulation can be broadly attributed to three causes: 1) lack of representative foliage or understory spectra; 2) inaccuracies due to simplification or misrepresentation of physical reality while creating the inputs for the FRT model or via the associated allometric models (e.g., estimation of crown dimensions from tree diameter and height); and 3) the simplifications of the radiative transfer computations in FRT. We combined the last two causes into a generic modelling error component. Thus, we conceptualized two broad FRT error causes: 1) insufficient spectral data, 2) modelling errors. We then designed an analysis to partition the error magnitude between these two causes. For this, we defined the following sets of observations.

- *All*: This consists of all observations available to us, irrespective of forest type, forest plot location or month of Landsat image acquisition. This consists of 17,573 observations derived from 12,369 unique forest plots. The months associated with these observations ranged from May to October.
- *SpectrallyMatched*: Here, we identified a subset of set *All* for which the spectral data used as input to the FRT model is well-matched with the actual spectra of the various elements associated with the plot (i.e., foliage, understory). Specifically, we only included observations for which: 1) the plots were from the Pirkanmaa region in Southern Finland (where our input needle and understory spectra were collected); 2) the fertility class were OMT and MT types (which is well-represented in our measured spectra); 3) the Landsat image was collected during summer, thus matching the season of the understory spectra. In all, 634 observations qualified for this set, representing 548 plots including ones from seedling stands and mixed stands.
- *SpectrallyMatched_StructurallySimple*: This is a subset of *SpectrallyMatched*, where we apply two more conditions: 1) The plot consisted of even-sized trees of a single species (number of strata is 1), and, 2) they were mature stands (*volume* $\geq$ 100 $m^3\,ha^{-1}$). In this set, there were 84 observations based on 77 unique forest plots.

Table 3
Random effects considered for the models.

Random effect	Description
plotID	FFC plot ID. Unique to each temporary plot created.
clusterID	Unique ID of the cluster that the plot is part of.
imageID	Unique ID of the Landsat image.
provinceName	The name of the administrative province containing the plot.

Table 4
Number of forest plots associated with each trajectory shown in Fig. 4.

Trajectory (volume category)	Pine	Spruce	Birch
Less than 20 $m^3\,ha^{-1}$	21	17	10
Between 20 and 100 $m^3\,ha^{-1}$	50	28	29
Greater than 100 $m^3\,ha^{-1}$	149	82	40

These represent plots where the forest canopy is more amenable to be well represented in FRT.

We then determined the RMSEs associated with each of the three sets given above. First, consider the sets *All* and *SpectrallyMatched* and their associated RMSEs. The decrease in RMSE between set *All* and set *SpectrallyMatched* roughly quantifies the benefit of well-representative spectra. That is, it quantifies the benefit the FRT framework would have, given that representative field spectra are available for the entire study area, and over all seasons of the year. Similarly, when one compares *SpectrallyMatched* and *SpectrallyMatched_StructurallySimple*, the difference in RMSEs roughly quantifies the inaccuracy due to FRT's simplification of vegetation structure, for young and mixed stands (i.e., in *SpectrallyMatched*). Hence, the relative decrease in bias and RMSE between *SpectrallyMatched* and *SpectrallyMatched_StructurallySimple* quantifies the effect of such simplification on the RMSE statistics.

3. Results

3.1. BRF estimation accuracy

FRT has a general tendency towards overestimation of BRF values compared with Landsat (Fig. 1), especially for birch-dominated plots. All these overestimations were found to be statistically significant. The magnitude of these overestimations are less in the visible bands (green and red) and more in the NIR and SWIR1 bands. The model performs best in the case of pine and spruce dominated plots, and for the green and red bands. This can be inferred by examining the bias and RMSE statistics associated with each subfigure of Fig. 1 (Fig. 2). Fig. 2 shows that the bias of FRT simulated BRFs range from a low of ~0.008 to a high of ~0.08. RMSE values range from a minimum of ~0.01 to a maximum of ~0.09. The magnitude of the estimated error is the smallest in the visible bands.

We generated two scatterplots of two representative subfigures from Fig. 1, to understand and illustrate the effect of stand maturity on BRF

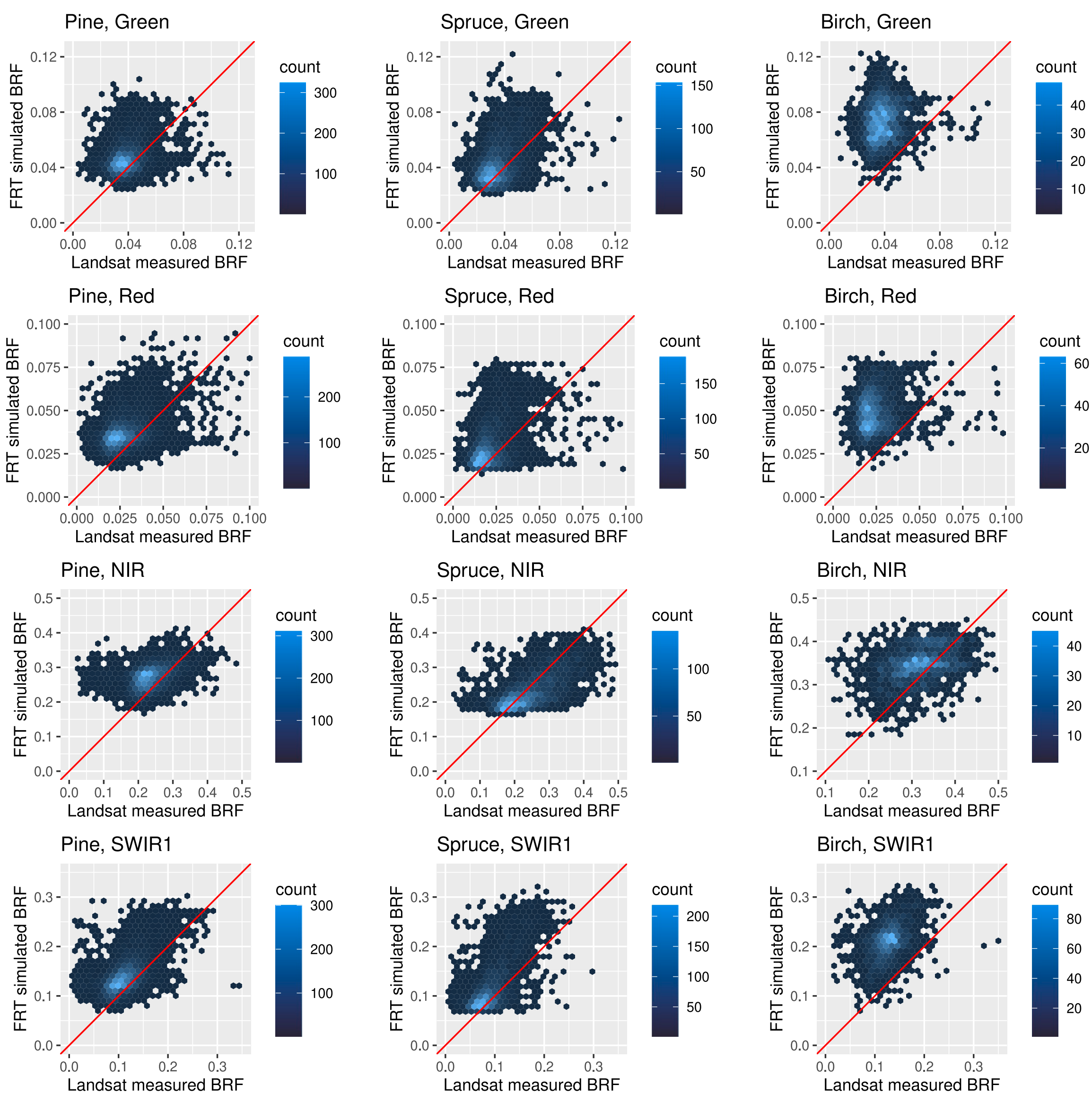

Fig. 1. Scatterplots of FRT simulated BRFs versus Landsat-measured ones, for the summer months. Each colored point in the scatterplot represents an observation, count indicates the number of observations represented by that colour. The dominant tree species of the forest plot and the Landsat 8 OLI band (Green, Red, NIR, SWIR1) is indicated at the top of each scatterplot. (For interpretation of the references to colour in this figure legend, the reader is referred to the Web version of this article.)

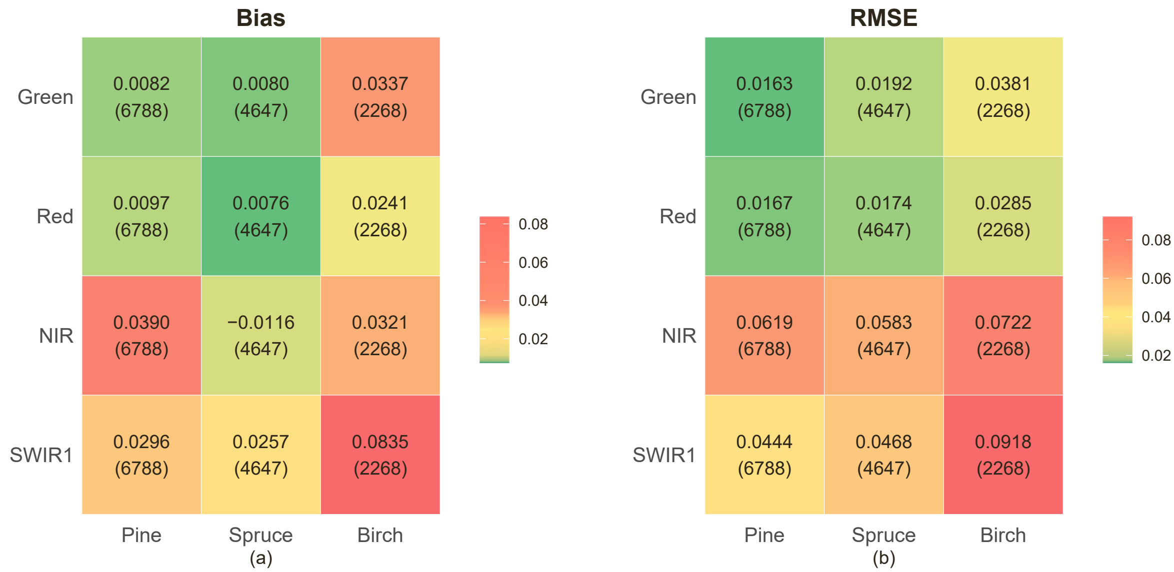

Fig. 2. Bias and RMSE statistics associated with subfigures of Fig. 1: each colored square above is associated with a subfigure of Fig. 1. For example, a bias of 0.0082 (top left corner, above) is associated with the "pine, green" scatterplot subfigure of Fig. 1. The number inside the brackets is the number of observations for the statistic. The colour of the squares helps identify low and high values: green colour indicates the lowest *absolute* value among the 12 associated squares, while red colour indicates the highest absolute value. (For interpretation of the references to colour in this figure legend, the reader is referred to the Web version of this article.)

simulation error (Fig. 3). There, one can notice that most observations farther away from the 1:1 line were associated with forest plots with low timber volumes (i.e., young stands). These tend to be overestimations of simulated BRF by FRT.

FRT seems to be moderately capable of reproducing temporal BRF trajectories of mature pine and spruce stands, in the green and red bands (Fig. 4). The observed similarities in the trajectories mostly persist, even after factoring in the confidence interval of these curves (Fig. S1). For example, when one considers the red band in Fig. 4, and for plots dominated by pine and spruce, the FRT and Landsat curves corresponding to the highest volume class (blue curves) are almost coincident with each other. Again, in the case of the NIR band for these two species, the two higher-volume associated FRT trajectories reproduce the general shape of the Landsat-based trajectories. For the low-volume case (sapling and young stands), there is a general trend of overestimation by FRT. Hence here (as in Fig. 3) we see that FRT agrees better with Landsat based BRF values for mature stands and less so for younger stands. Again, all the trajectories in Fig. 4 are generally more co-incident during the summer months. It can also be seen that in some cases, the temporal trends in BRF over the six months was hardly reproduced by FRT, e.g., the NIR band.

Fig. 3. Scatterplots of FRT simulated BRFs versus those measured via Landsat 8 OLI, for the summer months and for pine and birch dominated plots (red band) (two subplots of Fig. 1). Each colored point in the scatterplot represents a distinct observation. The dominant species of the forest plot and the Landsat band (Green, Red, NIR, SWIR1) are indicated at the top of each scatterplot. Categories of the timber volume of the plot (V) is also indicated. (For interpretation of the references to colour in this figure legend, the reader is referred to the Web version of this article.)

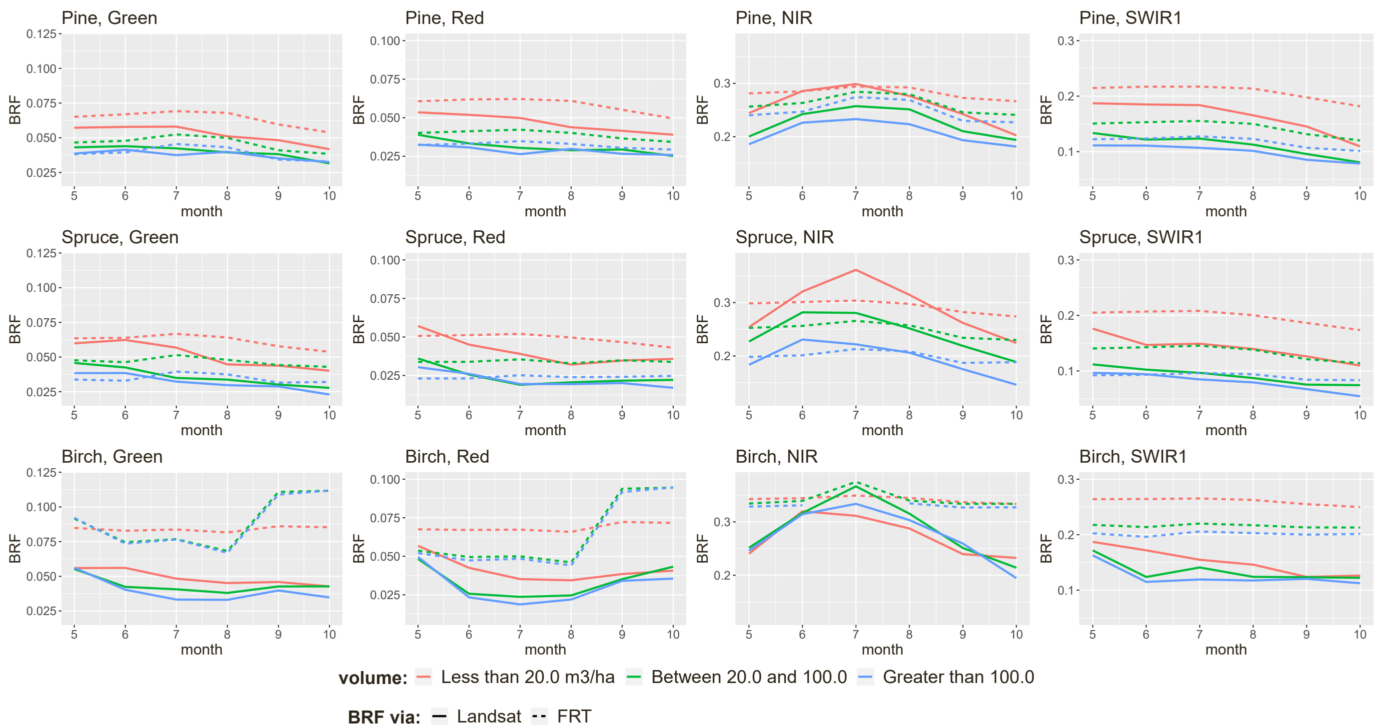

Fig. 4. The monthly trends of BRF simulated by FRT together with the measured curves from Landsat observations. The month ranges from May (5) to October (10). The dominant species of the forest plot and the Landsat band are indicated at the top of each graph. The number of plots associated with each trajectory line of the figure can be seen in Table 4.

3.2. Mean error

Our mixed model based analysis indicates that 27% of the variance of the error red band was explained by the fixed effects (the marginal R^2 of the model mod. meanerr.red is 0.27) and as much as 79% of the variance was explained by the combination of fixed and random effects (the conditional R^2 of the model mod. meanerr.red is 0.79). For the mixed model for mean error in the NIR band, mod. meanerr.NIR, the marginal and conditional l R^2 values are 0.19 and 0.65, respectively. The fixed effects used in the final models (mod.meanerr.red, mod. meanerr.NIR) along with their coefficient values are given in Table S3.

The dominant tree species of the plot and the season of the year were the most important factors influencing the magnitude of the error in the red band (Fig. 5). The set of fixed effects and their interactions in both formulated models (mod.meanerr.red, mod. meanerr.NIR; Table S3) can be split up into two distinct factor sets: 1) tree species, fertility class, and

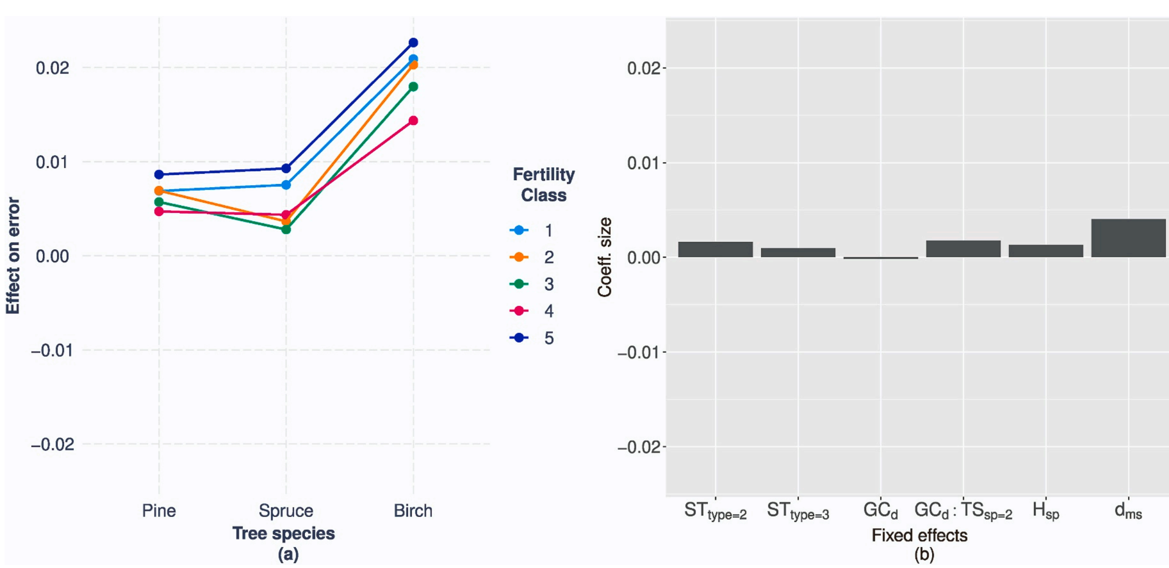

Fig. 5. Comparison of the various components of the mixed model for mean error, red band (mod.meanerr.red). (a) Interaction plot of tree species (TS) and fertility class (FC) on error seen. (b) Estimates of the other fixed effect coefficients. The categorical variable SG_{birch} (spectral group for birch), coefficient value 0.0368 in the mixed model is left out from the figure, because it is only applicable to a small subset of observations. The y-axis of (a) and (b) above are of the same scale, and hence the effect of error of each variable is intercomparable. (For interpretation of the references to colour in this figure legend, the reader is referred to the Web version of this article.)

their interactions; 2) the rest of the variables, like soil type, timber volume and the Gini coefficient. The relative contribution to the mean error of red band as per these two sets in the mod. meanerr.red model is shown in Fig. 5. Fig. 5(a) shows the effect of interaction of tree species and fertility class, when all other factors are held at such levels that they do not contribute to the error. Significant stand-alone effects are seen for tree species (TS) and fertility class (FC), along with only slight interaction effects between the two. Hence, the tree species is the most important factor; the simulated BRF values are most overestimated when the plot is dominated by birch or other broad-leaved species. This is seen across all fertility classes too. Smaller, but still consequential overestimations can be seen with pine and spruce plots too. BRF overestimation magnitude increases with increase in several other variables (Fig. 5(b)). The most important of them is the time of year (d_{ms}); the large and positive value of the coefficient implies that observations from latter parts of the year are associated with higher levels of overestimations. Soil-types 2 and 3 (spruce bog, pine bog) are associated with increased overestimations, when compared to mineral soils. The importance of tree-level heterogeneity can also be seen: plots with more tree size heterogeneity (GC_d) and tree species diversity (H_{sp}) tend to have higher over-estimations by FRT. We see that plotID and imageID are significant random effects (Table 5); together, they explain ~70% of the variance left over after accounting for the fixed effects.

Tree species, soil type and timber volume are the most important factors influencing the magnitude of error observed in the NIR band (Fig. 6). The components of figure are similar to those of Fig. 5. That is, it illustrates the magnitude of the coefficients of the mean error in the NIR band model (mod.meanerr.NIR) as per two sets of factors (see above). Tree species and fertility class showed small interaction effects between them, along with significant stand alone effects (Fig. 6(a)). Birch and pine dominated plots are associated with relatively large BRF overestimations. Meanwhile, FRT underestimates BRF for spruce dominated plots with fertility class 5 (poorest fertility). Most other fixed effect variables considered are associated with overestimations, except for tree size heterogeneity (GC_d) (Fig. 6(b)). Unlike the model for the error in the red band, the timber volume (V) is also shown to be important in this model. Higher timber volumes are associated with overestimations of NIR band reflectance.

Certain individual forest plots and Landsat images are associated with more BRF simulation error magnitudes than others (Table 5). Both plotID and imageID are important random effects; as much as 42% residual variance is explained by imageID for the red band. Meanwhile, the plot cluster does not have much explanatory power (associated value is ~5%).

3.3. *Relative contribution of spectral and geometrical components*

We had defined three distinct set of observations in an effort to separate out the contribution of spectral and geometrical components of the FRT framework to the observed error (see section 2.8). Considerable differences in RMSE statistics are seen between the sets *All*, *SpectrallyMatched* and *SpectrallyMatched_StructurallySimple* (Fig. 7). The percent decrease in RMSE when switching from set *All* to set *SpectrallyMatched* is seen in part (a) of the figure. The RMSE associated with the red band BRFs of spruce dominated forest plots drops by as much as 32%, when one compares such plots between sets *SpectrallyMatched* and *All* (there were 315 spruce-dominated plot observations in the set *SpectrallyMatched*). The median drop in RMSE seen in Fig. 7(a) is 17.8%, and most percent decrease values are in the range of 20–30%. This implies that as much as 20–30% of RMSE in a typical FRT simulation (i.e., set *All*) is due to the use of non-representative spectra, for our study area. The associated median statistics of Fig. 7(b) implies that an additional ~ 5% of RMSE of a typical FRT simulation can be reduced, given better geometric representations of reality in the FRT model.

Table 5
Percent residual variance explained by random effects in the two mixed effects models formulated.

Random effect	mod.meanerr.red	mod.meanerr.NIR
plotID	29.9	28.7
clusterID	NA	5.4
imageID	41.9	22.7

4. Discussion

4.1. *General considerations*

In this article, we quantified the accuracy of the FRT reflectance simulation model using data (12,369 forest plots) from an operational forest inventory database and corresponding satellite imagery spread over six months. The FFC forest plot data is publicly available and freely downloadable, which supports the repeatability of our set of experiments. Hence, the current effort represents a significant improvement over other FRT-related accuracy quantification efforts, due to this relatively larger geographical and seasonal coverage. Our results indicate that FRT seems to be relatively capable of simulating the Landsat BRF values for a sizable fraction (65%) of the cases (Figs. 1–4). That is, bias values as low as 0.01–0.03 and RMSE values as low as 0.02–0.05 were observed over a large number (~11,500) of observations over pine and spruce dominated plots, in the red and NIR bands (Fig. 3). This represents ~65% of the 17,573 observations we considered. As a reference for comparison, Rautiainen and Stenberg (2005) had compared BRFs simulated by the PARAS forest radiative transfer model with Landsat observations, using 800 forest stands. They reported RMSEs in the order of 0.1 units for the red band and 0.05 units for the NIR band. Discrepancies of similar order of magnitude were reported between the compared models for these two bands, in the latest round of RAMI model validation exercises (Widlowski et al., 2015). These statistics show that FRT compares well with other similar models for some cases, thus highlighting its overall potential. Meanwhile, RMSEs on the higher side (as high as 0.03 to 0.09) can also be see in Fig. 2, which shows the need for further work to improve the framework.

4.2. *Factors explaining FRT simulation inaccuracy*

We used a mixed modelling framework to attribute and understand the relative importance of the causes for the observed discrepancies (i.e., error) between FRT simulated and satellite BRFs. We envision that such analyses would help the FRT developers to better focus their efforts for improving the FRT simulation framework. The model for mean error in red band (mod.meanerr.red) helps us understand the relative importance of several variables related to the forest plot and date of image acquisition (Fig. 5). Tree species is identified as the most important variable. The time of the year (d_{ms}) is also identified as an important factor that determines the magnitude and direction of the error; this implies the importance of having representative spectra for all months of the year. This can also be a consequence of our assumption that the canopy LAI remains constant for all months considered, especially for birch dominated plots. Important implications of the model for mean error in NIR band (mod.meanerr.NIR) can be deduced from Fig. 6. The tree species is decisive here too: the BRF is considerably overestimated in pine and birch dominated plots. Tree size heterogeneity and timber volume are also shown to be important variables.

To roughly partition the error magnitude between that caused by non-representative spectra and that from geometric representation issues, we had defined three sets of observations: *All*, *SpectrallyMatched*, *SpectrallyMatched_StructurallySimple*. The reduction in RMSEs associated with the two latter sets (Fig. 7) implies that implies that ~20–30% of the RMSE of set *All* is attributable to non-representative spectra. Further, a 5% of RMSE seems to be related to geometric representation issues in the FRT model. The pattern of colours of the squares of the figure further

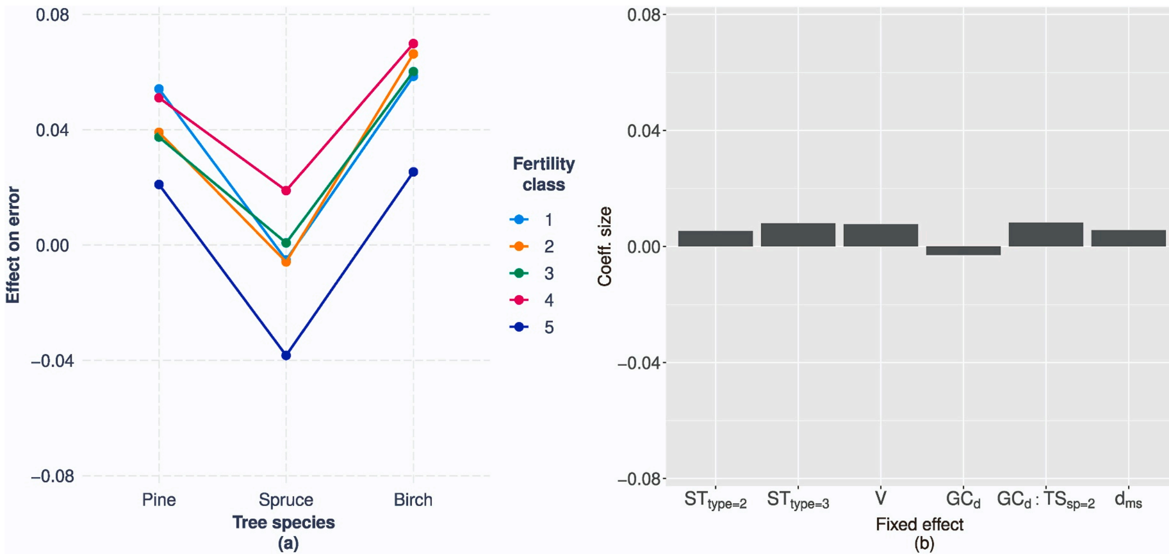

Fig. 6. The components of the mixed model for mean error in NIR band (mod.meanerr.NIR): a) interaction plot of the tree species (TS) and fertility class (FC) on error in the red and NIR bands; b) estimates of the other fixed effect coefficients. (For interpretation of the references to colour in this figure legend, the reader is referred to the Web version of this article.)

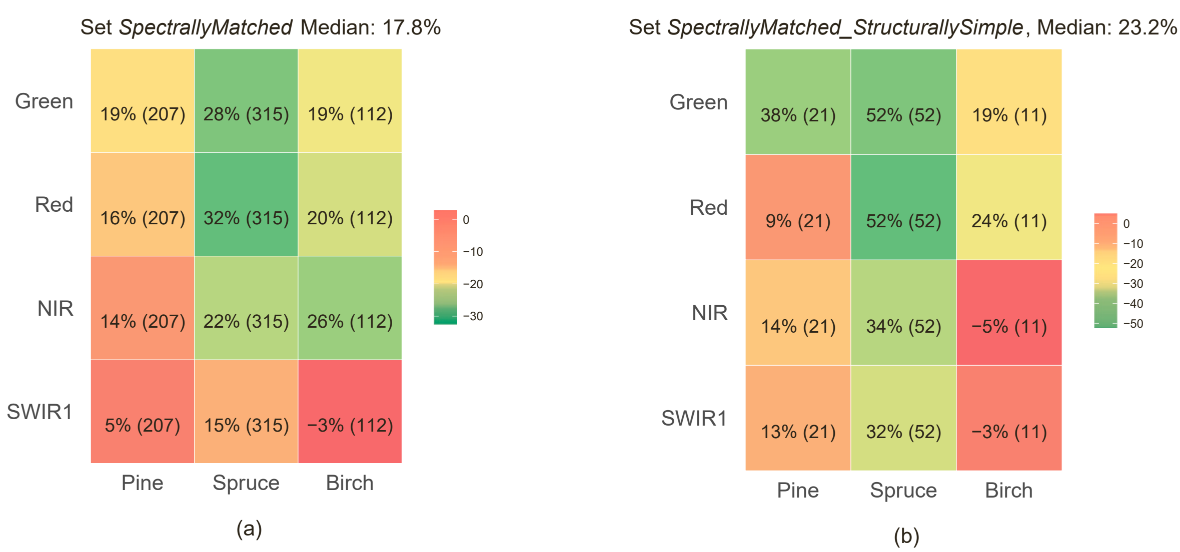

Fig. 7. Per-species and per-band decrease in RMSE (%) associated with the set, when compared to set *All*. The numbers inside the brackets are the number of observations associated with that statistic in the set. The colour of the squares helps identify low and high values: green colour indicates the highest (%) value among the 12 associated squares, while red indicates the lowest value. (a) Decrease in RMSE (%) associated with set *SpectrallyMatched*, when compared to set *All*. (b) Decrease in RMSE (%) associated with set *SpectrallyMatched_StructurallySimple*, when compared to set *All*. For an expanded version of this figure, see Fig. S2. (For interpretation of the references to colour in this figure legend, the reader is referred to the Web version of this article.)

indicate that spruce stands are most affected by these two issues, and especially for the green and red bands.

4.3. Importance of tree species, understory type and tree size heterogeneity

The tree species, the fertility class and their interactive effects were the most important factors explaining the mean error and its variance (Figs. 5 and 6). Fig. 5 indicates that the most important factor is tree species as per the mixed model mod. meanerr.red: it can increase the mean error by as much as 0.01 units. Tree species is an important driving factor of forest reflectance or albedo (Knyazikhin et al., 2013; Kuusinen et al., 2014). Kuusinen et al. (2014) reports that in middle aged or mature forests, forest albedo is influenced more by tree species composition than even Leaf Area Index (LAI) or canopy cover. Again, in birch and other broad-leaved (deciduous) stands, the forest floor dominates the total reflectance during the early and latter parts of the year. Thus, for these plots, uncertainties in the understory spectrum are more manifest in the plot-level reflectance values. We also found that several other variables such as soil type, tree size heterogeneity, species diversity and volume affect the error magnitude in the red and NIR bands.

Some fertility classes were associated with higher levels of BRF overestimations in some mixed models; e.g., class 1 and 5 in the red band and class 4 in the NIR band (Figs. 5 and 6). In general, the spectral-directional scattering behavior exhibited at the understory level of Fennoscandian forests can be very different, depending on the species present (Forsström et al., 2021). Again, the composition of the forest floor can depend on the overstory tree density; a previous work had found out that there was a 33% correlation between them (Majasalmi and Rautiainen, 2020). Temporally resolved seasonal understory spectra are also lacking. For a good discussion about the challenges of modelling understory elements in BRF simulations (birch stands), see Rautiainen et al. (2009).

Our models implied that stand-level tree class heterogeneity, both in terms of size classes and species, was an important source of error (Figs. 5 and 6). Spruce plots with unequal-sized trees are especially prone towards FRT overestimations in the NIR band. This may be partly due to the fact that we assumed all trees in a stratum to have the same size as the median tree. Meanwhile, plots that are more diverse species-wise (i.e., mixed forests) tend to have more error (Figs. 5 and 6), this is mostly because the internal representation of these stands in FRT diverges fairly from reality.

4.4. Satellite derived reference BRFs

We have used Landsat derived BRF estimates as our reference values. But for many cases, the satellite estimated BRFs may deviate from the true BRFs at the land surface. We found that imageID was an important random effect in both our mixed models: it explained 41.9% and 22.7% of the residual variance for the red and NIR band models, respectively (Table 5). The implication is that some Landsat images were associated with relatively higher error magnitudes than others. This further suggests the need for better atmospheric correction in the Landsat surface reflectance product. Our analysis of some associated satellite images suggests that cloud-wisps could be a source of error; they are sometimes flagged as “clear” pixels in the Landsat surface reflectance product. Generating good cloud masks is problematic and is an active area of research. For a recent intercomparison study of several such algorithms and the challenges that still remain, see Skakun et al. (2022). Uncorrected satellite measurements correspond to hemispherical directional reflectance factor (HDRF) values (Schaepman-Strub et al., 2006). Even though HDRF and BRF values are near-identical in some forested land covers (Schaepman-Strub et al., 2006, Fig. 4), scattering and shading effects of nearby terrain, vegetation and water bodies can be hard to account for and correct.

4.5. Future avenues of related work

The above analysis and our results from mixed models suggest that a promising future avenue of improvement of the FRT framework is increasing the representativeness of the field spectra.

Specifically, we recommend that the following spectra be collected.

1. On mineral soils: Collecting understory spectra for very fertile (OMaT) site (class 1), CT (class 5) and VT (class 4) sites should be a priority, as they are associated with higher levels of BRF overestimations. In Fig. 6(a), the lack of representative VT spectra coupled with the relative transparency of the canopy for this band is most probably the reason for overestimation associated with this fertility class. This fertility class represents over 22% of plots in our study area.
2. On peatlands: Understory spectra should also be collected for the peatlands, i.e., soil type 2 and 3; the associated coefficients are relatively large in Figs. 5(b) and 6(b).
3. Better seasonal spectra for the months of May, September and October (both foliage and understory) would also be useful. This statement is supported by the fact that the coefficient associated with the number of days to midsummer (d_{ms}) was positive and relatively large the two mixed models formulated. When examining the models further, we can gather that hence the error increases significantly as the date of satellite images advances beyond the midsummer, keeping all other factors constant. The trajectories seen in Fig. 4 also suggest the inadequate nature of spectra for months outside the summer period; i.e., May, September and October.

We observed that plotID was an important random effect for both mixed models formulated for mean error (Table 5). This implies that certain forest plots had specific characteristics that could not be captured by the current FRT framework. This could be related to the size class, structure, distribution of trees or vegetation present, or the terrain topography. Young stands were clearly associated with more error (Fig. 3) and improvements regarding their representation in FRT should be considered. High levels of error associated with some plots could also be related to the fact that the FFC plot and the Landsat pixel are of different shape and size, which might affect some plots more than others. Regular geometrical objects like ellipsoids, as used by FRT, may not capture the geometry of many tree crowns, which tend to be irregular. Previous work with FRT has shown the dependence of stand reflectance on tree crown shape (Rautiainen et al., 2004). These geometrical objects may not also capture the branching structure of trees, which may be pronounced and irregular in natural and old-growth forests. The contribution of woody elements such as tree trunks and first order branches to tree-level reflectance was quantified in a recent publication by Kuusinen et al. (2021), and it was estimated to vary between 0.09 and 0.2. Also, crown length and crown radius may not be well estimated in some cases by allometric equations. The representation of the spatial pattern of tree locations in the stand may not always be a realistic either. Further analysis of selected plots on these lines would be helpful to improving the FRT framework further and is a promising future avenue of work.

It is extremely challenging to develop a robust reflectance model for real-world forested conditions. This is because of the highly complex set of interactions that electromagnetic radiation can undergo, between the sun and the sensor. Nevertheless, our results indicate that FRT is capable of reproducing BRF values over a proportion of forest plot observations, given snow-free conditions. They also suggest that an augmented spectral library would result in considerable improvement of the simulation framework; such a library is relatively straightforward to incorporate into FRT. This includes the spectra of all elements of vegetation: leaf, needle, stem bark, branch bark and ground vegetation. All of these further suggest that FRT might be ultimately integrated into a forest management planning system, so that the albedo could be used as a criterion in forest management planning, and albedo-related radiative forcing could be quantified and factored in. In this case, simulated BRF studied in this article could be replaced by simulated albedo. There are significant climatic benefits in managing boreal forests considering albedo too (Bright et al., 2014). The reflectance model, in this case, should be able to realistically replicate the changes in albedo introduced by different forest management operations. But there are several significant challenges to overcome before such an integration into a forest management system happens, and we briefly touch upon some of them here. First, the managed forest stands of southern Finland are not necessarily representative of such managed or natural forests in other regions of the boreal zone. Thus, an exercise like this should be repeated with a much wider sampling of forest plot set, to identify further avenues for improvement of the FRT framework. Secondly, the model framework should be verified and extended for snow-laden months. There have been previous efforts that have attempted to factor in albedo into forest management decisions (Sjølie et al., 2013; Lutz and Howarth, 2014) but they were mostly of coarse-scale or confined to the temperate region. Third, there is the challenge of verification of the model for fully diffused lighting conditions, such as cloudy and hazy days. Again, the impact of terrain slope and topography has to be studied, before application to more mountainous areas. Additional work with respect to computational efficiency is also needed before incorporation FRT framework into a forest planning system. A library of precomputed albedo values as a function of forest attributes and a look-at-table type search could be a reasonable and fast solution in the simulation-optimization systems used in forest planning.

5. Conclusions

This study provides a broad picture of the performance of the Forest Reflectance and Transmittance model in reproducing observed reflectances over a wide variety of forest types. It is shown that FRT can reproduce observed reflectances over a proportion (65%) of observations considered. These are predominantly for mature forests, i.e., where the forest structure is relatively simple and representative input spectra are also available. However, it fails to adequately reproduce the observed BRFs for sizable fraction of the simulated cases, especially for young stands and for non-summer months. We also studied broad seasonal trends in BRF and ascertained that FRT can generally reproduce such trends for mature forest stands, and to a lesser extend for younger stands. We used a set of mixed models to attribute the cause of the discrepancies observed to various factors. The results of these analyses provide guidance to future model improvement efforts. Previous work has shown that FRT is applicable to boreal regions outside Finland. Hence improvements to the FRT and the input data used by the model coupled with wider-region verification efforts would lead to more accurate reflectance modelling for a geographically wide area. The necessity to collate more geographically and temporally comprehensive spectral libraries is important to the larger community of radiative transfer modelers as it holds for any physically based reflectance model. We also recommend improving the representation of reality in forest reflectance models, such as developing better associated forest allometric models. Both these efforts will be advantageous to the general reflectance modelling community.

6. Code and data availability

The FFC forest plot data is publicly available and can be downloaded from the website (Metsäkeskus, 2022). The Google Earth engine JavaScript code for extracting plot-level surface reflectance values and the C++ code for generating FRT input files are available on RJee007 Github repository: https://github.com/RJee007. The fortran code for the specific version of the FRT used in the studies is available from the authors via e-mail request. Later FRT versions are available under the LGPL license.

Declaration of competing interest

The authors declare that they have no known competing financial interests or personal relationships that could have appeared to influence the work reported in this paper.

Data availability

I have a "code and data availability" section where I provide details where one can get a copy of the relevant computer code & data.

Acknowledgements

We acknowledge funding for this work from the Academy of Finland (grant number 317741 for the OPTIMAM project, grant number 337127 for the UNITE flagship, grant number 317387 for the AIROBEST project, grant number 348152 for the ARTISDIG project). A. Hovi and M. Rautiainen received funding from the European Research Council (ERC) under the European Union's Horizon 2020 research and innovation programme (grant agreement No 771049). The text reflects only the authors' view, and the Agency is not responsible for any use that may be made of the information it contains. We would also like to thank Dr. Roope Ruotsalainen for sharing his code related to some R/ggplot figures.

Appendix A. Supplementary data

Supplementary data to this article can be found online at https://doi.org/10.1016/j.srs.2023.100098.

References

Barsi, J.A., Lee, K., Kvaran, G., Markham, B.L., Pedelty, J.A., 2014. The spectral response of the Landsat-8 operational land imager. Rem. Sens. 6, 10232–10251.
Bright, R.M., Antón-Fernández, C., Astrup, R., Cherubini, F., Kvalevåg, M., Strømman, A. H., 2014. Climate change implications of shifting forest management strategy in a boreal forest ecosystem of Norway. Global Change Biol. 20, 607–621.
Chen, F., 2005. Variability in global land surface energy budgets during 1987–1988 simulated by an off-line land surface model. Clim. Dynam. 24, 667–684.
Darvishzadeh, R., Skidmore, A., Abdullah, H., Cherenet, E., Ali, A., Wang, T., Nieuwenhuis, W., Heurich, M., Vrieling, A., O'Connor, B., 2019. Mapping leaf chlorophyll content from Sentinel-2 and RapidEye data in spruce stands using the invertible forest reflectance model. Int. J. Appl. Earth Obs. Geoinf. 79, 58–70.
Disney, M.I., Lewis, P.E., Bouvet, M., Prieto-Blanco, A., Hancock, S., 2009. Quantifying surface reflectivity for spaceborne lidar via two independent methods. IEEE Trans. Geosci. Rem. Sens. 47, 3262–3271.
Douglas Bates, M.M., Bolker, B., Walker, S., 2015. Fitting linear mixed-effects models using lme4. J. Stat. Software 67, 1–48.
Forsström, P.R., Juola, J., Rautiainen, M., 2021. Relationships between understory spectra and fractional cover in northern European boreal forests. Agric. For. Meteorol. 308, 108604.
Forster, P., Ramaswamy, V., Artaxo, P., Berntsen, T., Betts, R., Fahey, D.W., Haywood, J., Lean, J., Lowe, D.C., Myhre, G., 2007. Changes in atmospheric constituents and in radiative forcing. In: Climate Change 2007. The Physical Science Basis (Chapter 2).
Gorelick, N., Hancher, M., Dixon, M., Ilyushchenko, S., Thau, D., Moore, R., 2017. Google earth engine: planetary-scale geospatial analysis for everyone. Rem. Sens. Environ. 202, 18–27.
Hadi, Rautiainen, M., 2018. A study on the drivers of canopy reflectance variability in a boreal forest. Remote Sensing Letters 9, 666–675.
Hovi, A., Liang, J., Korhonen, L., Kobayashi, H., Rautiainen, M., 2016. Quantifying the missing link between forest albedo and productivity in the boreal zone. Biogeosciences 13, 6015–6030.
Hovi, A., Raitio, P., Rautiainen, M., 2017. A spectral analysis of 25 boreal tree species. Silva Fenn. 51, 7753.
Jones, H.G., Vaughan, R.A., 2010. Remote Sensing of Vegetation: Principles, Techniques, and Applications. Oxford university press.
Knyazikhin, Y., Martonchik, J.V., Myneni, R.B., Diner, D.J., Running, S.W., 1998. Synergistic algorithm for estimating vegetation canopy leaf area index and fraction of absorbed photosynthetically active radiation from MODIS and MISR data. J. Geophys. Res. Atmos. 103, 32257–32275.
Knyazikhin, Y., Schull, M.A., Stenberg, P., Mõttus, M., Rautiainen, M., Yang, Y., Marshak, A., Latorre Carmona, P., Kaufmann, R.K., Lewis, P., 2013. Hyperspectral remote sensing of foliar nitrogen content. Proc. Natl. Acad. Sci. USA 110, E185–E192.
Kuusinen, N., Hovi, A., Rautiainen, M., 2021. Contribution of woody elements to tree level reflectance in boreal forests. Silva Fenn. 55.
Kuusinen, N., Lukeš, P., Stenberg, P., Levula, J., Nikinmaa, E., Berninger, F., 2014. Measured and modelled albedos in Finnish boreal forest stands of different species, structure and understory. Ecol. Model. 284, 10–18.
Kuusk, A., Kuusk, J., Lang, M., 2014. Modeling directional forest reflectance with the hybrid type forest reflectance model FRT. Rem. Sens. Environ. 149, 196–204.
Kuusk, A., Nilson, T., 2000. A directional multispectral forest reflectance model. Rem. Sens. Environ. 72, 244–252.
Kuusk, A., Nilson, T., Paas, M., Lang, M., Kuusk, J., 2008. Validation of the forest radiative transfer model FRT. Rem. Sens. Environ. 112, 51–58.
Lutz, D.A., Howarth, R.B., 2014. Valuing albedo as an ecosystem service: implications for forest management. Climatic Change 124, 53–63.
Majasalmi, T., Rautiainen, M., 2020. The impact of tree canopy structure on understory variation in a boreal forest. For. Ecol. Manag. 466, 118100.
Maltamo, M., Packalen, P., 2014. Species-specific management inventory in Finland. In: Forestry Applications of Airborne Laser Scanning. Springer, pp. 241–252.
Mehtätalo, L., Lappi, J., 2020. Biometry for Forestry and Environmental Data: with Examples in R. Chapman and Hall/CRC.
Metsäkeskus (spatial data, in Finnish) [WWW Document] 2022. Metsäkeskus. URL https://www.metsakeskus.fi/fi/avoin-metsa-ja-luontotieto/aineistot-paikkatieto-ohjelmille/paikkatietoaineistot (accessed 18 August 2023).
Mõttus, M., Stenberg, P., Rautiainen, M., 2007. Photon recollision probability in heterogeneous forest canopies: compatibility with a hybrid GO model. J. Geophys. Res. Atmos. 112.
Muinonen, E., 1995. Metsikön heijastussuhteen ennustaminen geometrisella latvustomallilla. Licenciate of Science thesis (in Finnish). University of Joensuu, Faculty of Forest Sciences.
Nakagawa, S., Schielzeth, H., 2013. A general and simple method for obtaining R2 from generalized linear mixed-effects models. Methods Ecol. Evol. 4, 133–142.
Natural Resources Canada, 2021. The State of Canada's Forests Annual Report. https://www.nrcan.gc.ca/our-natural-resources/forests/state-canadas-forests-report/16496. (Accessed 18 August 2023).
Natural Resources Institute Finland, 2018. Forest Statistics. https://stat.luke.fi/en/. (Accessed 18 August 2023).

Nilson, T., Peterson, U., 1991. A forest canopy reflectance model and a test case. Rem. Sens. Environ. 37, 131–142.

Oksanen, J., Blanchet, F.G., Friendly, M., Kindt, R., Legendre, P., McGlinn, D., Minchin, P., O'Hara, R., Simpson, G., Solymos, P., et al., 2022. vegan: Community Ecology Package. R package version 2.5–7. 2020.

Pinheiro, J., Bates, D., 2006. Mixed-effects Models in S and S-PLUS. Springer science & business media.

Rautiainen, M., Lang, M., Mõttus, M., Kuusk, A., Nilson, T., Kuusk, J., Lükk, T., 2008. Multi-angular reflectance properties of a hemiboreal forest: an analysis using CHRIS PROBA data. Rem. Sens. Environ. 112, 2627–2642.

Rautiainen, M., Lukeš, P., 2015. Spectral contribution of understory to forest reflectance in a boreal site: an analysis of EO-1 Hyperion data. Rem. Sens. Environ. 171, 98–104.

Rautiainen, M., Mõttus, M., Heiskanen, J., Akujärvi, A., Majasalmi, T., Stenberg, P., 2011. Seasonal reflectance dynamics of common understory types in a northern European boreal forest. Rem. Sens. Environ. 115, 3020–3028.

Rautiainen, M., Nilson, T., Lükk, T., 2009. Seasonal reflectance trends of hemiboreal birch forests. Rem. Sens. Environ. 113, 805–815.

Rautiainen, M., Stenberg, P., 2005. Application of photon recollision probability in coniferous canopy reflectance simulations. Rem. Sens. Environ. 96, 98–107.

Rautiainen, M., Stenberg, P., Nilson, T., Kuusk, A., 2004. The effect of crown shape on the reflectance of coniferous stands. Rem. Sens. Environ. 89, 41–52.

Reda, I., Andreas, A., 2004. Solar position algorithm for solar radiation applications. Sol. Energy 76, 577–589.

Repola, J., 2008. Biomass equations for birch in Finland. Silva Fenn. 42, 605–624.

Repola, J., 2009. Biomass equations for Scots pine and Norway spruce in Finland. Silva Fenn. 43, 625–647.

Roy, D.P., Wulder, M.A., Loveland, T.R., Woodcock, C.E., Allen, R.G., Anderson, M.C., Helder, D., Irons, J.R., Johnson, D.M., Kennedy, R., 2014. Landsat-8: science and product vision for terrestrial global change research. Rem. Sens. Environ. 145, 154–172.

Schaepman-Strub, G., Schaepman, M.E., Painter, T.H., Dangel, S., Martonchik, J.V., 2006. Reflectance quantities in optical remote sensing—definitions and case studies. Rem. Sens. Environ. 103, 27–42.

Sjølie, H.K., Latta, G.S., Solberg, B., 2013. Potential impact of albedo incorporation in boreal forest sector climate change policy effectiveness. Clim. Pol. 13, 665–679.

Skakun, S., Wevers, J., Brockmann, C., Doxani, G., Aleksandrov, M., Batič, M., Frantz, D., Gascon, F., Gómez-Chova, L., Hagolle, O., 2022. Cloud Mask Intercomparison eXercise (CMIX): an evaluation of cloud masking algorithms for Landsat 8 and Sentinel-2. Rem. Sens. Environ. 274, 112990.

Townsend, P.A., Serbin, S.P., Kruger, E.L., Gamon, J.A., 2013. Disentangling the contribution of biological and physical properties of leaves and canopies in imaging spectroscopy data. Proc. Natl. Acad. Sci. USA 110. E1074–E1074.

USGS, 2020. Landsat 8 Collection 1 Land Surface Reflectance Code Product Guide. U.S. Geological Survey [WWW Document]. URL. https://www.usgs.gov/media/files/landsat-8-collection-1-land-surface-reflectance-code-product-guide. (Accessed 18 August 2023).

Vermote, E., Justice, C., Claverie, M., Franch, B., 2016. Preliminary analysis of the performance of the Landsat 8/OLI land surface reflectance product. Rem. Sens. Environ. 185, 46–56.

Widlowski, J.-L., Mio, C., Disney, M., Adams, J., Andredakis, I., Atzberger, C., Brennan, J., Busetto, L., Chelle, M., Ceccherini, G., 2015. The fourth phase of the radiative transfer model intercomparison (RAMI) exercise: actual canopy scenarios and conformity testing. Rem. Sens. Environ. 169, 418–437.

Widlowski, J.-L., Taberner, M., Pinty, B., Bruniquel-Pinel, V., Disney, M., Fernandes, R., Gastellu-Etchegorry, J.-P., Gobron, N., Kuusk, A., Lavergne, T., 2007. Third radiation transfer model intercomparison (RAMI) exercise: documenting progress in canopy reflectance models. J. Geophys. Res. Atmos. 112.

Yang, G., Zhao, C., Liu, Q., Huang, W., Wang, J., 2010. Inversion of a radiative transfer model for estimating forest LAI from multisource and multiangular optical remote sensing data. IEEE Trans. Geosci. Rem. Sens. 49, 988–1000.

Zeileis, A., Kleiber, C., 2014. Ineq: measuring inequality, concentration, and poverty. R package version 0.2-13, URL. http://CRAN.R-project.org/package=ineq. Accessed on 25th August 2023.